Effect of rotary swaging on structure and properties of low-carbon steel

IOP Conf. Series: Materials Science and Engineering **848** (2020) 012092 doi:10.1088/1757-899X/848/1/012092

Effect of rotary swaging on structure and properties of low-carbon steel

A A Tokar [1,5*], V A Lunev [1,5], A S Dolzhenko[2], O V Rybalchenko[1,5], M M Morozov[1], V S Yusupov[1], G V Rybalchenko[3], P D Odessky[4] and S V Dobatkin[1,5]

[1] A A Baikov Institute of Metallurgy and Materials Science of RAS, Leninsky prospect, 49, 119991, Moscow, Russia
[2] Belgorod State University, Pobeda st., 85, Belgorod, 308015, Russia
[3] P.N. Lebedev Physical Institute of RAS, Leninsky prospect, 53,119334 Moscow, Russia
[3] V A Kucherenko TSNIISK, 2nd Institutskaya, 6, 109428, Moscow, Russia
[4] National University of Science and Technology "MISIS", Leninsky prospect, 4, 119991, Moscow, Russia

*E-mail: tokarb2005@mail.ru

Abstract. The structural transformation and mechanical properties of a low-carbon 0.2% C steel and a 0.09% C–Mn–V steel in coarse- and ultrafine-grained (UFG) states were studied. The UFG structure with structural elements about 210-375 nm in size was obtained by rotary swaging (RS) and equal-channel angular pressing (ECAP). ECAP was used to compare the influence of the industrial deformation and SPD methods on the microstructure and properties of low-carbon steels. It was shown that an increase in true strain ratio and a decrease in final temperature of RS improve strength properties and reduce plasticity of these steels. In both steels after RS, σ_{UTS} within the range from 800 up to 920 MPa with elongation in the range of 15-17% at the final deformation temperature of 400 °C was obtained. It was found that the strength of 0.2% C steel after ECAP was on the same level with that steel after RS. The strength properties of low- carbon 0.09% C–Mn–V steel after ECAP were significantly higher than those after RS.

1. Introduction

Severe plastic deformation (SPD) methods lead to significant refinement of the microstructure and improve the strength and service properties of low-carbon steels [1,2]. The ultrafine-grained low-carbon steels were already obtained by such methods as equal-channel angular pressing (ECAP) [2-6] and high pressure torsion (HPT) [7-9]. However, these methods are hard to implement in industry. One of the industrial deformation schemes used, for example, in the automotive industry, is rotary swaging (RS) [10]. This method allows the molding of pipes, rods and wires to give the final shape to the deformed parts with minimal subsequent processing or without it. This technique was already approved for refinement of the microstructure of many alloys [11, 12].

Usually the unalloyed or low-alloyed low-carbon steels are subjected to severe plastic deformation in the initial ferritic-pearlitic state. The initial ferritic-pearlitic structure is convenient for SPD process since it does not need high deforming force. However, the obtained microstructure after deformation is

inhomogeneous and unstable during heating. On the other hand, the initial martensitic state provides a more dispersed microstructure and better strengthening than initially ferritic–pearlitic state [9,13]. Additionally, the formation of a fine carbide phase after quenching leads to increased thermal stability of such a microstructure. However, the deformation process of the initial martensitic structure requires increased deforming force. In our study we use high-temperature tempering of the steels after quenching. Such thermal treatment will secure uniform distribution of carbides after quenching and reduce the deforming force owing to high-temperature tempering.

The aim of present study is to evaluate the UFG microstructure that obtained by the RS method in the low-carbon steels and to clarify the difference between the microstructures processed by RS and SPD methods. The microstructure and thermal stability of strengthening of low-carbon 0.2% C steel and 0.09% C–Mn–V steels is studied and the effect of UFG structure of these steels on its mechanical behaviour is determined.

2. Experimental

The chemical compositions of the low-carbon 0.2% C and 0.09% C–Mn–V steels are shown in Table 1. The high-temperature treatment was performed by 2 regimes: (1) quenching at a temperature of 880°C (holding time of 1 h followed by water cooling) and tempering at a temperature of 600°C (holding time of 1 h) for the 0.2% C steel; (2) quenching at a temperature of 920°C (holding time of 1 h followed by water cooling) and tempering at 680°C (holding time of 1 h) for the 0.09% C–Mn–V steel. The microstructures of these steels in the initial state after quenching and high-temperature tempering are shown in figure 1.

Table 1. Chemical composition of steels.

Steels	Amount (wt.%)											
	C	Mn	Si	Ni	Mo	V	Cu	Cr	P	S	As	Fe
0.09% C–Mn–V	0.096	1.56	0.19	0.1	0.0027	0.05	0.13	0.12	0.02	0.014		balance
0.2% C	0.19	0.21	0.49	0.03			0.19	0.25			0.05	balance

RS was realized by a rotary swaging (RS) machine RKM 2129.02 (figure 2 a). Billets of 19.6 mm in diameter and 100 mm in length were deformed by RS machine with the frequency and magnitude of the impacts of the dies of 1920 min^{-1} and 3 mm, respectively. Eight impacts of dies per one revolution about the axis were applied to the billet [11, 12]. RS was carried out via two RS regimes with a stepwise decrease in the temperature of deformation within the range from 650 °C to 500 °C, or from 600 °C to 400 °C. The true stain increased from 0.6 to 2.3 during RS. The true stain (ε) was estimated by the formula:

$$\varepsilon = \ln(\mu),$$

where μ – is the total extrusion ratio equal to A_0 / A_f, where A_0 and A_f are the initial and the final cross-sectional area of the billets, respectively [11, 12].

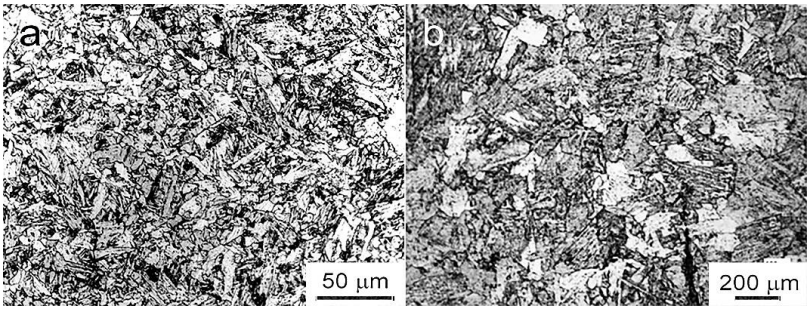

Figure 1. Light micrographs of the microstructure of 0.09% C – Mn – V (a) and 0.2% C (b) steels after quenching and high-temperature tempering.

ECAP (figure 2 b) of the specimens of 20 mm in diameter and 80 mm in length was carried out at a temperature of 400°C by route Bc (successive axial rotation of the billet by 90° after each pass). The intersection angle between the channels was 120°, and the numbers of passes N = 4 resulted in true strain of 3.6. The true strain applied to the billet per pass for the defined die geometry equals 0.9 (shear strain $\gamma = 1.5$) [14 ,15].

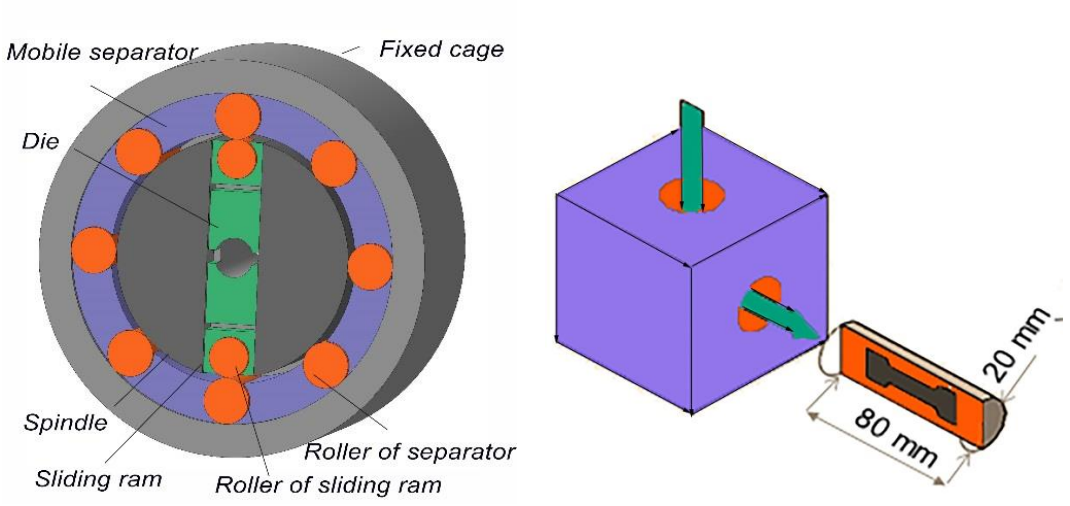

a b

Figure 2 Schemes of RS (a) and ECAP (b).

RS of the 0.09% C–Mn–V steel was performed in two regimes with a stepwise decrease in the deformation temperature of each stage: regime1: 1 stage at 650°C ($\varepsilon = 0.6$) → 2 stage at 575°C ($\varepsilon = 1.2$) → 3 stage at 500°C ($\varepsilon = 2.3$); and regime 2: 1 stage at 600°C ($\varepsilon = 0.6$) → 2 stage at 500°C ($\varepsilon = 1.2$) → 3 stage at 400°C ($\varepsilon = 2.3$). RS of the 0.2% C steel was performed by the regime 2.

The microstructure was analysed in optical Olympus PME 3 microscope and in JEM- 1400 transmission electron microscope. The samples for the metallographic analysis were chemically etched with a solution of 3% nitric acid in C_2H_5OH. Thin foils for transmission electron microscopy (TEM) were mechanically ground to 90 μm and thinned to perforation electrolytically with a supersaturated solution of chromic anhydride in orthophosphoric acid, at a voltage of ~23 V.

The mechanical properties were determined using a tensile testing INSTRON 3380 machine with a load capacity of 100 kN. Microhardness was measured on a 402 MVD Wolpert Wilson instrument at a load of 100g.

3. Results and Discussion

The light micrographs of microstructure of the 0.09% C–Mn–V steel after RS are shown in two regimes with a decrease in the deformation temperature in figure 3. The microstructure of the 0.09% C–Mn–V steel after 1 stage of 1 RS regime with a true strain of 0.6 doesn't differ from the initial microstructure of this steel (figure 1, figure 3a). The 2nd stage of 1 RS regime led to the oriented initial grain microstructure (figure 3b). As we can see from the light micrograph of samples, microstructure after the final 3 stage of the RS is significantly oriented (figure 3c).

The TEM analysis revealed the formation of a submicrocrystalline grain-subgrain microstructure with an average grain/subgrain size of 325±30 nm (figure 4). The average size of the microstructural elements was determined from dark-field TEM images (figure 4b). During RS the refinement of microstructure occurred due to formation of the shear bands with a thickness of about 300 nm and the formation of subgrains inside of them. Point reflections on an annular electron diffraction patterns in the corresponding TEM micrographs (the inset of figure 4a), as well as a fringe contrast at the grain boundaries (figure 4a) proved the presence of high-angle boundaries, i.e. the grain microstructure.

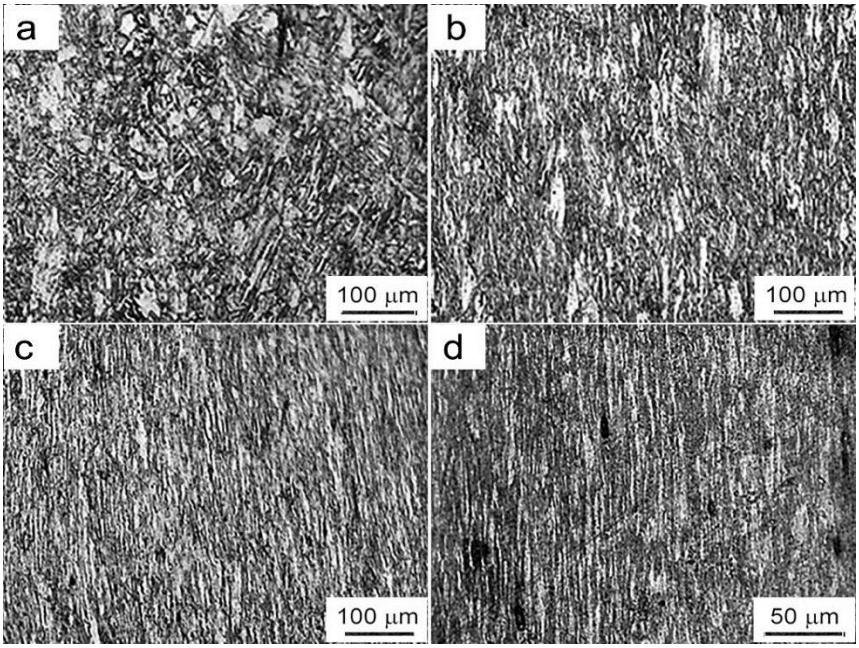

Figure 3. Light micrographs of the microstructure of 0.09% C–Mn–V steel after RS by 1 regime: stage 1 (a), stage 2 (b), stage 3 (c); 2 regime stage 3 (d)/

The metallographic analysis of the 0.09% C– Mn –V steel after the last stage of the second regime with a true strain of 2.3 revealed even more oriented microstructure comparing to that after 1 regime as a result of a lower final temperature (figure 3d).

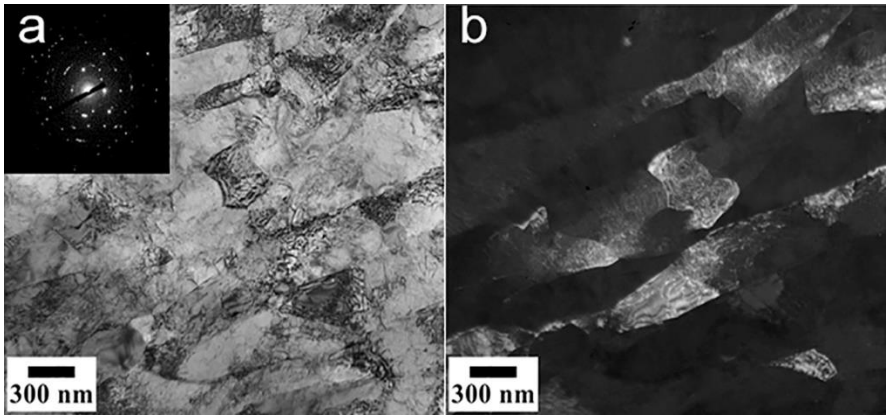

Figure 4. TEM micrographs and SAD pattern for a sample of 0.09% C–Mn–V steel after RS by 1 regime.

During RS by the second regime the refinement of 0.09% C–Mn–V steel microstructure also occurred due to the formation of the shear bands. The thickness of these shear bands is about 215±30 nm (figure 5). The TEM analysis revealed a small grain with an average size of 130 nm with a fringe contrast at the boundaries.

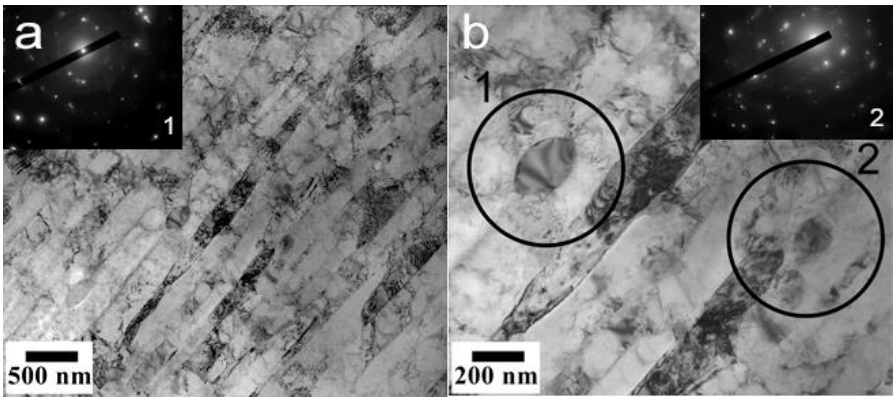

Figure 5. TEM micrographs and SAD patterns for a sample of 0.09% C–Mn–V steel after RS by 2 regime.

The TEM analysis of the 0.2% C steel after RS by the 2 regime also revealed a highly oriented structure (figure 6). Submicrocrystalline structure with an average grain size of 285 nm is seen in the TEM image.

Accordingly, the selected regimes of RS of the 0.2% C steel and the 0.09% C–Mn–V steel let to produce a predominantly UFG microstructure with grain sizes within the range of 285 - 375 nm. It should be noted that the subgrain structure of these steels was stabilized by the carbide phase precipitates.

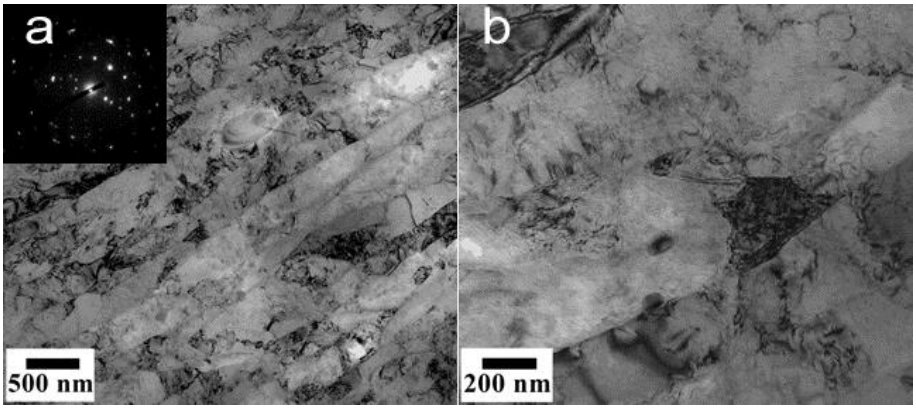

Figure 6. TEM micrographs and SAD pattern for a sample of 0.2% C steel after RS by 2 regime.

The TEM analysis of samples after ECAP doesn't reveal the formation of shear bands. The deformation subrgrains/grains have a quasi-equiaxial shape. The TEM micrographs of the samples after deformation by ECAP for a number of passes N = 4 showed a partially submicrocrystalline and, mostly, subgrain structure (figure 7). The high-angle misorientation of the boundaries is judged from the character of an annular electron diffraction patterns in the corresponding TEM micrographs (in the inset of figure 7) with individual point reflections, as well as a fringe contrast at the boundaries. The average size of the microstructure elements of the 0.2% C steel and the 0.09% C–Mn–V steel after ECAP is about 375± 30 nm and 209.4±19 nm, respectively. The grain refinement in the 0.2% C steel by ECAP was almost the same as that by RS. In contrast, the extent of refining the microstructure of the 0.09% C–Mn–V steel after ECAP was significantly higher than that after RS.

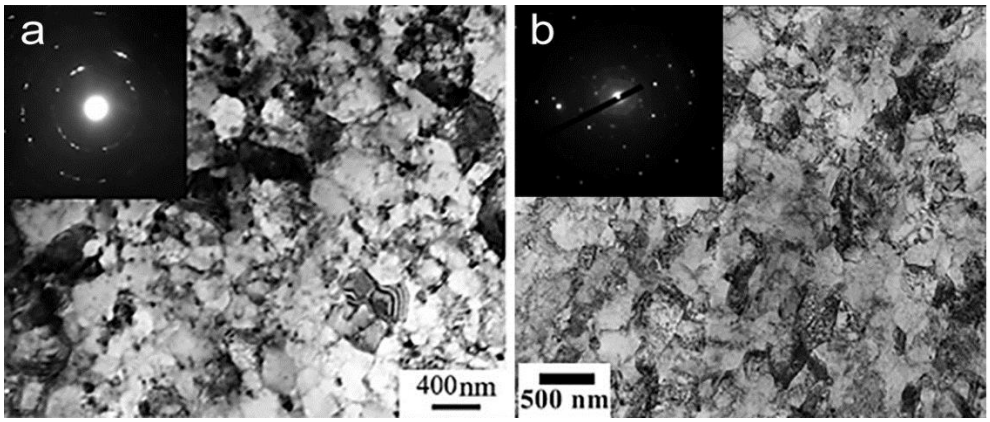

Figure 7. TEM micrographs and SAD patterns for the samples of 0.2% (a) and 0.09% C–Mn–V (b) steels after ECAP.

The thermal stability of strengthening of the 0.2% C steel and the 0.09% C–Mn–V steel after RS was studied according to the change in the microhardness during annealing. The values of microhardness increase with increasing the stage in each regime of RS (figure 8). After RS, the microhardness of the 0.09% C–Mn–V steel is higher as compared with that of 0.2% C steel (figure 8). The thermal stabilities of the 0.2% C steel and the 0.09% C–Mn–V steel after both regimes of RS are nearly the same. However, despite a significantly higher level of strengthening, the thermal stability of the samples after RS is lower than that after quenching and tempering.

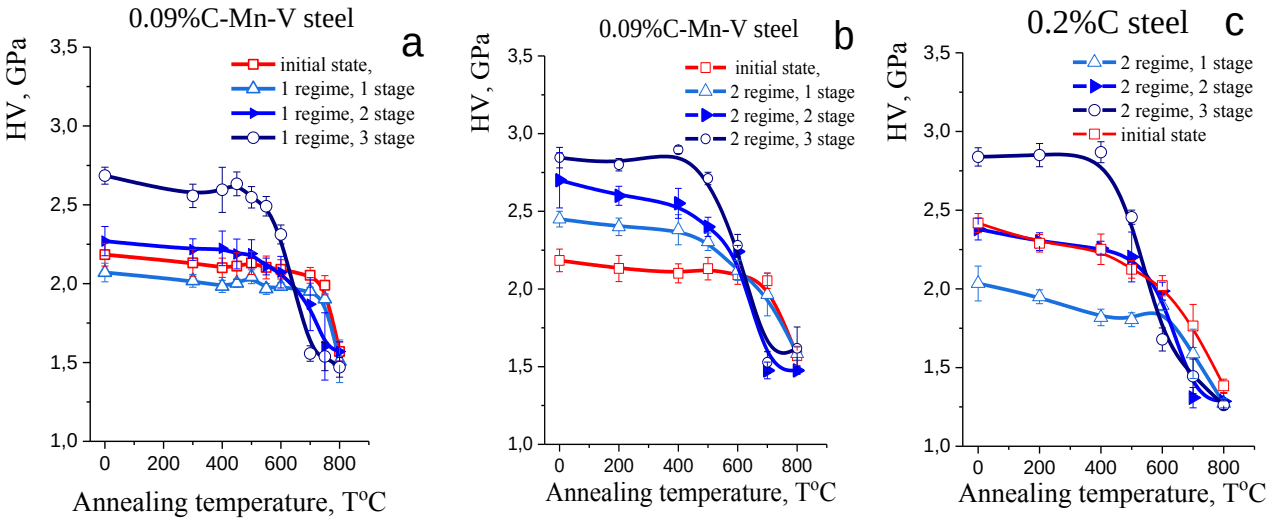

Figure 8. The thermal stability of 0.09% C–Mn–V (a, b) and 0.2% C (c) steels after RS by 1 regime (a) and 2 regime (b, c).

Comparing the strength properties of both steels deformed by the second regime, we can observe that RS at first stage with a true strain of 0.6 leads to a slightly higher σ_{UTS} of the 0.09% C–Mn–V steel and RS at the last stage with a true strain of 2.3 leads to a higher σ_{UTS} of the 0.2% C steel (figure 9, Table 2). It should be noted, however, that the values of σ_{UTS} of these steels are nearly the same. Consequently, σ_{UTS} in the range from 808 to 922 MPa was obtained for both steels at the final stage of RS with good elongation of δ = 16-17%.

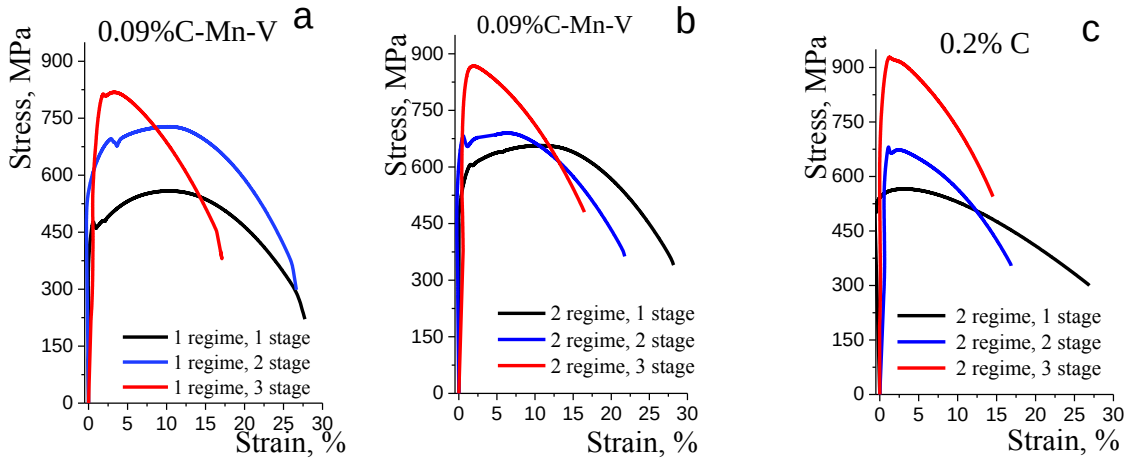

Figure 9. Mechanical properties of 0.09% C–Mn–V (a, b) and 0.2% C (c) steels after RS.

The strength properties of low- carbon 0.09% C–Mn–V steel after ECAP was significantly higher then those after RS (figure 10 a, Table 2). The ultimate strength of 0.2% C steel after ECAP was on the same level as that after RS (figure 10 b, Table 2). In contrast, the strength properties of low-carbon 0.09% C–Mn–V steel after ECAP are better then those after RS (figure 10), probably, because of the better structure refining and precipitation of fine special carbides during severe plastic deformation.

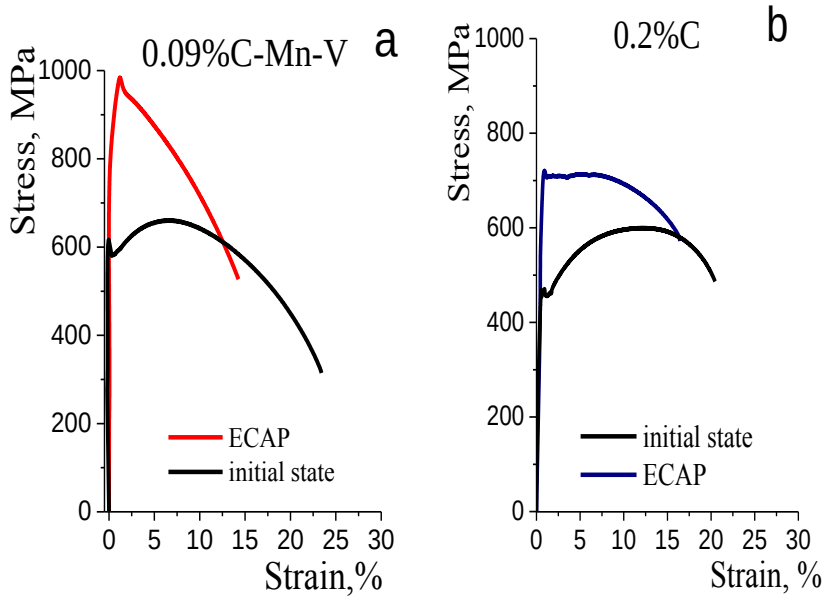

Figure 10. Mechanical properties of the 0.09% C–Mn–V steel (a) and the 0.2% C steel (b) after ECAP.

Table 2. Mechanical properties of 0.09% C–Mn–V and 0.2% C steels

Steels	Regime /stage,		σ_{UTS}, MPa	σ_{YS}, MPa	δ,%
0.09% C–Mn–V steel	Initial state		594	480.8	27
	RS	1 regime / 1 stage	558.4	460.4	28
		1 regime / 2 stage	727.8	678	26.6
		1 regime / 3 stage	818.5	808	17.1
		2 regime / 1 stage	653.9	603.8	28
		2 regime / 2 stage	689.6	654.2	21.8
		2 regime / 3 stage	866.7	846	16.5
	ECAP		984	940	14,3
0.2% C steel	Initial state		600	460	21
	RS	2 regime / 1 stage	565	504.6	27
		2 regime / 2 stage	672.7	664	16.9
		2 regime / 3 stage	927.4	922.6	14.5
	ECAP		742	730	16,4

4. Conclusions

The UFG microstructure evolution during RS in the low-carbon 0.2% C and 0.09% C–Mn–V steels was studied and the difference between the microstructures developed by RS and SPD methods was clarified.

1. The selected regimes of RS led to predominantly UFG microstructure in the 0.2% C steel and the 0.09% C–Mn–V steels with grain/subgrain sizes within the range of 285 - 375 nm.
2. The grain refinement in the 0.2% C by ECAP and RS was almost the same. However, refining the microstructure in the 0.09% C–Mn–V steel after ECAP was much pronounced than that after RS.
3. For both steels σ_{UTS} in the range from 800 to 920 MPa at admissible elongation of 16-17% were obtained at the final stage of RS.
4. The tensile strength of the low-carbon 0.2% C steel after ECAP does not exceed the tensile strength of this steel after RS at the final temperature. In contrast, the strength of the 0.09% C–Mn–V steel after ECAP significantly exceeds that after RS.

Acknowledgments

The work was carried out within the governmental task 075-00746-19-00 and supported by RFBR (grant 18-08-00321).

References

1. Valiev R Z, Zhilyaev A P, Langdon T G 2014 *Bulk nanostructured materials: Fundamentals and Applications* (New Jersey: TMS-Wiley).
2. Dobatkin S V 2000 *Investigations and Applications of Severe Plastic Deformation* (Dordrecht: Kluwer Academic) **3(80)** 13
3. Shin D H, Kim W-J, Choo W Y 1999 Scripta Mater .**41** 259
4. Park K-T, Shin D H 2002 Mater. Sci. Eng. A **334** 79
5. Shin D H, Kim W-J, Kim Y-S, and Park K-T 2000 *Acta Mater*. **48** 2247
6. Shin D H, Kim I, Kim J, and Park K T 2001 *Acta Mater*. **48** 1285
7. Astafurova E G, Dobatkin S V, Naidenkin E V et al. 2009 *Nanotechnologies in Russia* **4** 109
8. Degtyarev M V, Chashchukhina T I, Voronova L M et al. 2007 Acta Mater. **55** 6039
9. Dobatkin S V, Shagalina S V, Sleptsov O I, Krasilnikov N A 2006 *Russian Metallurgy* **5** 445
10. Radyuchenko Yu S 1962 *Rotary swaging. Processing of parts on rotary swaging crimping machines* (Moscow MASHGIZ) (in Russian).

11. Martynenko N S, Luk'yanova E A, Morozov M M et al. 2018 *Met. Sci. Heat Treat.* **60** (3-4) 253.
12. Martynenko N, Lukyanova E, Gorshenkov M et al. 2018 *Mater. Sci. Forum* **941** 808.
13. Sastry Sh M L, Dobatkin S V, Sidorova S V 2004 *Russian Metallurgy* **2** 129
14. Iwahashi Y, Horita Z, Nemoto M., Langdon T G 1997 *Acta Mater.* **45** 4733.
15. Iwahashi Y, Wang J, Horita Z, Nemoto M, Langdon T G 1996 *Scripta Mater.* **35 (2)** 143.